T. Ernst, S. Szidat, J. Handl, D. Jakob, R. Michel, Ch. Schnabel, H.-A. Synal, F.J. Santos Arevalo, I. Benne, J. Boess, E. Gehrt, A. Capelle, J. Schneider, W. Schäfer, J. Böttcher

Migration of iodine-129 and iodine-127 in soils

To draw the balance of anthropogenic ^{129}I input into European soils, the concentrations of ^{129}I and ^{127}I in seven soils from Lower Saxony were analyzed down to a depth of 250 cm. In comparison with pre-nuclear soils and Ukrainian soils, we detected a significant anthropogenic input of ^{129}I. Considering the different time periods for the input of ^{129}I and ^{127}I it was possible to assess the dynamics of sorption processes which dominate migration and accumulation. Anthropogenic ^{129}I was successfully used as a tracer for a clarification of the migration processes of trace elements in soils.

Migration von Iod-129 und Iod-127 in Böden

Zur Bilanzierung des anthropogenen ^{129}I-Eintrages in europäische Böden wurden sieben niedersächsische Böden bis zu einer maximalen Tiefe von 250 cm auf ihre ^{129}I- und ^{127}I-Gehalte untersucht. Es konnte ein deutlich belegbarer Eintrag von anthropogenem ^{129}I durch Vergleiche mit pränuklearen Böden und ukrainischen Böden ermittelt werden. Unter Berücksichtigung der unterschiedlichen Eintragszeiträume für ^{129}I und ^{127}I konnte die Dynamik der Sorptionsprozesse, die Migration und Akkumulation dominieren, beurteilt werden. Damit ist es gelungen, den anthropogenen ^{129}I-Eintrag als Tracer zur Klärung der Migration von Spurenstoffen in Böden zu nutzen.

1 Introduction

The long-lived radionuclide ^{129}I ($T_{1/2}$ = 15.7 Ma) occurs naturally in the environment as a consequence of galactic cosmic ray interactions with xenon in the atmosphere and of spontaneous fission in the lithosphere. In atmosphere, hydrosphere, and biosphere it mixes with stable ^{127}I. The resulting natural pre-nuclear $^{129}I/^{127}I$ ratio was found to be 1.5×10^{-12} [1] and $(1.4 \pm 0.9) \times 10^{-12}$ [2] in recent oceanic sediments and in deep oceanic water, respectively. The pre-nuclear $^{129}I/^{127}I$ ratio is the result of long mixing times with small production and disintegration rates, which entails in the equilibration of both nuclides. The global natural abundance of ^{129}I was estimated to be 50 Mg (327 TBq), with a free inventory in atmosphere, hydrosphere, and biosphere of 263 kg (1.7 TBq) [3]. The free ^{129}I is exchanged between the environmental compartments with turn-over times of less than 1000 years. Man-made ^{129}I released by atmospheric explosions of nuclear weapons, by the Chernobyl accident and, most important, by emissions from reprocessing plants have increased the natural isotopic $^{129}I/^{127}I$ ratios by several orders of magnitude. Today, ^{127}I and ^{129}I are no longer in equilibrium in the environmental compartments [4].

In print: Kerntechnik 68 (2003) 4

This work deals with an investigation of deposition and migration of iodine isotopes in soils from Lower Saxony. Migration is the movement of atoms from the surface into the deeper layers of the soil as consequence of various transporting processes. The processes resulting in the migration may also contribute to an accumulation of the atoms in certain layers of the soil. Accumulation of a substance, contained in precipitation and consequently transported into the soil water as dissolved material, as particulate matter or as colloids, is an increase of its concentration in the water-unsaturated zone (upper soil) by evaporation of water. The evaporation process forces the water to move into the opposite direction of the migration, without the latter being excluded (see chapter 5.2). Diffusion boundary layers, which are formed from adsorbed water and capillary water at the soil matrix, contribute to the accumulation. Isotope effects can be neglected for all migration, accumulation and isotopic exchange processes. The differences in the apparent migration behavior between ^{127}I and ^{129}I observed in this work (see chapter 4) can be explained on the basis of the probabilities of sorption. In this sense it is certainly correct that there is just a small part of ^{127}I in the soil which shows identical migration behavior as ^{129}I. It is this small part of ^{127}I which has been deposited on the soil since 1940 together with the ^{129}I. This recent amount of ^{127}I is so small that it is not relevant for the migration of the total quantity of ^{127}I. In our investigation, only the total amount of ^{127}I in the soil samples is measured. As a consequence, there is an apparently different migration behavior of the trace material (here ^{129}I) compared to a material (^{127}I) with substantially higher concentration and with identical chemical and physical characteristics.

The results presented here are part of a long-term project aimed at the investigation of the radioecology of ^{129}I and the implementation of ^{129}I as an environmental tracer [4 - 6]. From earlier investigations [5, 6] it is known that Lower Saxony is exposed to a continuous fall-out of ^{129}I with an annual deposition density of up to 19 mBq m^{-2}. The $^{129}I/^{127}I$ ratios in precipitation increased from 1×10^{-9} in the 1950s up to 1.7×10^{-7} in 1986 in Central Europe and after a short maximum as a consequence of the Chernobyl accident the ratios stayed nearly constant with a value of $\sim 6.5 \times 10^{-7}$ [5].

2 Sampling and sample characteristics

Samples from soil profiles were taken at seven locations in Lower Saxony, Germany (Fig. 1), in connection with the preparation of soil-scientific excursions of the German Soil Science Society 1999 [7]. Trenches were freshly excavated and the soil samples were taken immediately from the walls of these trenches. The samples were stored in plastic bottles in the dark at temperatures below 20°C before analysis.

The different sampling locations are well distinguishable in terms of their particular soil characteristics. Their soil properties can be used to interpret the observed differences in the migration of the iodine isotopes. For such a discussion, all parameters have to be considered which affect the evapotranspiration and the hydrodynamic dispersion. The hydrodynamic dispersion is caused by molecular diffusion and depends on the grain and pore size distributions. It results in a high variability with depth of the distribution of traces [16]. Important parameters of the texture are the concentrations of clay (< 0.002 mm), silt (0.002 mm up to 0.063 mm), and sand (0.063 mm up

to 2 mm) in the humus-free fine soil fraction (< 2 mm). Moreover, the concentrations of carbon, nitrogen and the pH values [7] were considered in the discussion of the migration behavior (cmp. chapter 4).

3 Analysis

The soil samples were air-dried in the dark at room temperature. They were milled and thereafter sieved through a 2 mm mesh sieve and the bulk densities of the air-dried samples were determined in order to allow the calculation of deposition densities. Though the analyses were performed on the air-dried samples, all data given in this report refer to sample masses of oven-dried samples (105 °C for 1 hour). A tracer controlled iodine-matrix separation was performed before the measurement of ^{129}I by accelerator mass spectrometry (AMS) was carried out. Because AMS is a relative counting method, the ^{127}I concentrations were analyzed separately by ion chromatography (IC) to determine the intrinsic ^{129}I/^{127}I ratios in the samples. For the iodine-matrix separation a dry combustion method with excess oxygen was used collecting the iodine in the combustion gasses in an alkaline hydrosulphite solution [3]. For that purpose two telescoped quartz pipes were used with oxygen and nitrogen feed lines. In the inner pipe the pre-combustion was raised by smoldering in order to limit the production of combustion gasses and to avoid the samples to go up in flames. In the outer pipe, there was an oxygen overspill generated for the after-burning. For this a part of outer pipe reached into a tube furnace where the final combustion took place at 1120^{o}C. In order to increase the reaction time for combustion gasses quartz wool was used. The final combustion of the soil was realized by pushing the inner pipe into the tube furnace. The chemical yields of the iodine-matrix separations were determined using ^{125}I as tracer. Typical yields were between 80 % and 96 %. The chemical yields and the concentrations of ^{127}I and ^{129}I were determined with aliquots of the alkaline hydrosulphite solution. Before ^{129}I was determined with AMS, the iodine was precipitated with stable iodine carrier (Woodward iodine) as silver iodide. The intrinsic ^{129}I/^{127}I-ratio of the Woodward iodine is $(1.3 \pm 0.6) \times 10^{-14}$ [8] . The masses of the AgI precipitates were between 2 mg and 4 mg. The AgI was mixed with 20 mg silver and pressed into sample holders to be used as AMS-targets. The AMS measurements were performed at the PSI/ETH AMS facility at ETH Hönggerberg, Zurich. The ^{127}I concentrations were analyzed by an IC system (Dionex, Sunnyvale, USA) with AG5-/AS5-columes, auto-suppressor and conductivity detector. An optical method had a detection limit of 50 ng iodine g^{1} soil according to DIN 32 645 [6]. Typical detection limits for the ^{129}I/^{127}I-ratio were 5×10^{-12} (DIN 25 482 part 10) [6]. The ^{129}I blank values of the total analyses were determined with Woodward iodine as trace catcher. The blank ^{129}I/^{127}I ratios were in terms of geometric means and geometric standard deviations $(1.3 \times 2.0^{\pm1}) \times 10^{-12}$ and $(3.5 \times 1.7^{\pm1}) \times 10^{-13}$ for seven and eight blank analyses, respectively, performed in the two laboratories used.

4 Experimental results

The results of the measurements of ^{129}I and ^{127}I in the soil profiles are presented in tables 1 to 7. Preliminary results [9] had to be corrected for the case of ^{127}I concentrations in the field Twenge. In table 8 deposition densities of ^{129}I and ^{127}I are given which were calculated as surface projected activity or mass concentrations A_F according to equ. 1.

$$A_F = \int_{d_{max}}^{d_{min}} C(d) \cdot r(d)\, \mathrm{d}d \qquad \text{Eq. 1}$$

with d_{max} being the maximum sampling depth, d_{min} the depth of the top of the actual sampling interval, $C(d)$ the (activity or mass) concentration at depth d of ^{129}I and ^{127}I, respectively, and $r(d)$ the density of the soil at depth d. In the following, we frequently make use of these surface-projected ^{127}I and ^{129}I mass or activity concentrations in units of g m^{-2} and mBq m^{-2}, respectively, i.e. the concentrations projected onto the surface of the sampling interval. For these projections the bulk densities of the air-dried soil specimens were used. The ^{127}I and ^{129}I concentrations or activity concentrations measured in the samples comprise all those atoms, which at the time of sampling were bound to the soil matrix and those which were contained in the water contained in the soil. Loss of iodine from the soil moisture can be excluded because of the careful sample preparation.

The ^{129}I activity concentrations of the soils were between (267 ± 11) nBq g^{-1} and (1413 ± 46) nBq g^{-1} at the surface and between (3.51 ± 0.14) nBq g^{-1} and (0.76 ± 0.09) nBq g^{-1} in the deepest layers investigated. The ^{127}I concentrations ranged from (2.5 ± 0.1) mg kg^{-1} to (5.6 ± 0.4) mg kg^{-1} at the surface and from (1.60 ± 0,08) mg kg^{-1} to 0.06 mg kg^{-1} in depth. The ^{129}I/^{127}I isotopic ratios were 10^{-7} to 10^{-8} at the surface (Fig. 2). At depths the isotopic ratios showed much more variability ranging from 5×10^{-11} to 10^{-8}. The lowest isotopic ratios at depth thus exceeded the pre-nuclear marine equilibrium ratios by nearly 2 orders of magnitude and the lowest ratio measured so far a pre-nuclear soil $(5.7 \pm 1.1) \times 10^{-12}$ [6] by more than one order of magnitude.

Neither the depth profiles of the ^{129}I/^{127}I isotopic ratios (Fig. 2) nor the surface projected ^{127}I and ^{129}I concentrations as a function of d_{max} (Fig. 3) can be translated into the time dependence of the fallout because the soil characteristics dominate the behavior of ^{129}I and ^{127}I migration and consequently the ^{129}I/^{127}I ratios. The ^{129}I/^{127}I ratios at the surface are about two orders of magnitude smaller than in the precipitation [5, 6], i.e. the ^{129}I/^{127}I ratios are lowered in the top soils by dilution with stable ^{127}I already present before. The ^{129}I/^{127}I ratios do not show monotonous dependence on depth. Apparently, ^{129}I and ^{127}I differ in their migration behavior. But this is an artifact as a consequence of the competition in the migration of trace amounts of ^{129}I and ^{127}I from recent fallout with the large amount of ^{127}I being in the soil already for long times. It is striking that if one looks for the sequence of the soils on the basis of the iodine concentrations, the sequence of depth profiles of surface projected concentrations of ^{127}I does not correspond with that of ^{129}I (comp. Fig. 3 ^{129}I and ^{127}I). A model of the migration of the two iodine species must explain this apparently differing behavior taking into consideration the soil characteristics. As a basis for the discussion of the accumulation and migration mechanisms the soil characteristics will therefore be described in some detail in the context of the experimental results for all seven soil.

4.1 Pasture Vestrup

The pasture Vestrup [7, p. 191-192] is a dystric planosol, somewhat poorly drained with a moderately deep lying damming body. The parent material is aeolian (boulder) sand above boulder

clay. The pH value is between 5.3 and 4.3. For detailed characteristics of the soil profiles and for the experimental data see table 1.

The soil is characterized by increasing concentrations of silt, clay, and of a more coherent structure with increasing depth (sintered up to cemented structure). The lower horizons (starting below 40 cm) show an pronounced plastic, clay-similar behavior, although the main part is sand. The hydrological condition of this soil is characterized by backwater below 40 cm (Sw-horizons), so that the vertical water through-flow is hindered. The transient area between upper and lower soil is characterized by illuvial horizons Bs and Bhs (around 30 cm).

In the backwater horizons (Sw-horizons) we observe no further decrease of the $^{129}I/^{127}I$ ratios. Similar conditions in the lower soil zones exist at the sampling location Eilenriede (boulder clay). However, the plastic properties are less expressed. Both soils, at Vestrup and Eilenriede, show high $^{129}I/^{127}I$ ratios increasing slowly with depth in the lower soil zones (Fig. 2). This is the result of particularly small ^{127}I concentrations (Fig. 3).

Despite a small downward water through-flow, a high rate of iodine migration is observed. This leads to higher ^{129}I concentrations in comparison with those of ^{127}I. The reason is that a part of the water is stored in the soil matrix. This part of the water is able to adsorb temporarily iodine isotopes in thermodynamically unstable states via physical adsorption. The stored water has lost its flow characteristics and miscibility with the rest of the water. It could be called dead water. For any water volume that enters these horizons, an equal volume must leave it to deeper depths for reasons of continuity without a chance for a dissolved material to interact with the soil matrix. The condition for this is sufficient availability of water which is demonstrated by the plastic properties of these horizons. The faster migration of the iodine isotopes lead to a prevalence of iodine from recent fall-out and consequently to higher $^{129}I/^{127}I$ ratios.

In the soil Vestrup, the high $^{129}I/^{127}I$ ratios in the top 20 cm are remarkable. Here, a highly effective evapotranspiration and, consequently, a more effective ^{129}I accumulation by capillary rise can be assumed due to a closed vegetation cover. The same holds true for the forest Eilenriede and the lawn Ricklingen (Fig. 2). The capillary rise rates increase with increasing clay concentration, compactness of the packing, and coherency of the structure [12]. Therefore, the evapotranspiration is highest in the soil Vestrup compared with the other soils investigated. The capillary rise occurs in those depth ranges of the soil in which noteworthy quantities of water can ascend against the gravitation potential. It determines the depth range over which migrated traces in the soils can ascend and can be accumulated [13].

4.2 Forest Eilenriede

The sampling location Eilenriede [7, p. 353-355/367-368] is a deciduous forest with a somewhat poorly drained stagni-eutric gleysol. The parent material is boulder clay on a substratum of moraine loam. The pH values were between 4.8 and 5.1. For detailed characteristics of the soil profile and for the experimental data see table 2.

This location has a closed vegetation cover. It is laying in a lowland sand valley with a high groundwater level (gleysol) and backwater (stagni-eutric gleysol) (Go-Sw-horizon). Therefore, the $^{129}I/^{127}I$ ratios decrease steeply with depth below the upper 30 cm. Also here an efficient accumulation is to be assumed. The accumulation results from the closed vegetation cover and the reaching suction in the root area without the deep roots of the trees. The low pH value of 4.8 indicates a restrained biological activity, so that less water-insoluble humic substances can be formed and water-soluble complexing agents are favored [17]. This results in a higher mobility of iodine, since organically bound iodine can be more easily transported by water.

4.3 Lawn Ricklingen

The sampling location Ricklingen [7, p. 353-355/363-364] is a lawn in a former graveyard. The soil is a stagnic-luvisol, with differences in clay concentrations of less than 5%. The parent material is sandy loess (70 cm to 120 cm) above fluvial sand. The pH values were between 6.5 and 6.7. For detailed characteristics of the soil profile and for the experimental data see table 3.

This location is a lawn on a city graveyard of Ricklingen which has not been used for burials up to now. It has a closed grass cover. The slightly acescent soil with a pH of 4.8 to 5.1 consists of sand loess over fluvial sand and is equal to a stagnic-luvisol. Vertical clay displacements are observed down to a depth of 65 cm (Al, respectively, At2 horizon). Below 65 cm first signs of an influence of backwater are seen. For this soil, there appears a clear transition between the accumulation underneath the closed vegetation cover and a flatter decrease of the $^{129}I/^{127}I$ ratios below which is normally observed in the upper soil zones of the fields investigated. Then, the $^{129}I/^{127}I$ ratios drop slowly in the illuvial horizons At2 and Bt. The decline of the $^{129}I/^{127}I$ ratios is – contrary to the soils Vestrup and Eilenriede – a result of a stronger decrease of the ^{129}I concentrations than those of ^{127}I (comp. Fig. 3 ^{129}I and ^{127}I). A similar ^{129}I migration behavior shows the soil Barum within the range from 50 cm to 100 cm depth.

4.4 Field Barum

The sampling location Barum [7, p. 209-211] is a field. The soil is a moderate cumulic anthrosol. It is very well drained. The parent material is a fluvial loess (50 cm) over sandy loess (1 m) over wind-borne sand over glacial fluvial sand on a substratum of fluvial loess over sand loess over abyssal wind-borne sand. The pH values ranged from 5.9 to 6.0. For detailed characteristics of the soil profile and for the experimental data see table 4.

Here, the soil structure causes a high usable field capacity, i.e. the amount of plant-available water. A fast drainage of excess water after precipitation leads to a fast interruption of the water conductivity into the lower soil zone [17]. There are clay enrichments at depths between 60 cm and 120 cm, which do, however, not lead to tailback of water. This is an important difference from the soil at Ricklingen. The ^{127}I concentrations at Ricklingen do not decrease as fast under the backwater influence than those in the soil Barum. At Barum, the ^{127}I concentrations decrease strongly at depths below 75 cm where a change takes place from clay silt to sand with few clay and medium sand. The fast discharge of seeping water within the depth range of 60 cm to 120 cm leads to an increase of the $^{129}I/^{127}I$ ratios. The band-like clay enrichment (Bt3) on top of the C-horizon (below 120 cm,

containing broken rocks) strengthens the horizontal water through-flow. Obviously, here an effective washing-out of migrated iodine takes place so that the $^{129}I/^{127}I$ ratios are more alike to those in the fallout of recent years. A similar increase of the $^{129}I/^{127}I$ ratios can be recognized in the lower soil zone of the sampling location Twenge.

4.5 Field Twenge

The sampling location Twenge [7, p. 334-335] is a field. The soil is a fimic anthrosol, moderately well drained. The parent material is a plaggic horizon above glacial fluvial sand. The pH values ranged from 4.2 to 4.7. For detailed characteristics of the soil profile and for the experimental data see table 5.

This original gleyic podzol was affected by laying out sods (grass pieces), which had been used before as floor-cover within stables. From this an nearly 40 cm thick intensely enriched humos plaggic horizon formed. The strongly acescent milieu is characteristic for a forest location. Down to 75 cm the soil is neither affected by backwater nor by groundwater. Due to the very small amounts of silt and clay and because of the low pH value large migration rates are expected. Correspondingly, the parallel ^{127}I depth dependences between 75 cm and 120 cm characterize the soil Twenge as the one with the smallest ^{127}I concentrations after Vestrup. Only the soil Barum shows a lower value at the surface of the deepest sampling taking interval (Twenge 0.06 ± 0.03 g cm^{-2}, Barum 0.02 ± 0.004 gcm^{-2}). While ^{127}I is intensively washed out in the soil Barum, this is not observed in the soil Twenge. But, at the deepest samples, the soils Eilenriede and Barum exhibited the same $^{129}I/^{127}I$ ratios of 2×10^{-9}. Obviously, the influence of the groundwater prevents a super-proportional decrease of the iodine concentrations within the soil Twenge. The enrichment of organic material, in the form of sods, can hardly be seen in the depth-profile of the $^{129}I/^{127}I$ ratios. But around 50 cm the $^{129}I/^{127}I$ ratios remain constant. This can be interpreted as an influence of the sods if one considers the observations made in the soil Adenstedt where also organic inclusions are present at about 40 cm depth.

4.6 Field Adenstedt

The sampling location Adenstedt [7, p. 262-263] is a field with crop rotation of wheat, wheat, sugar beets. The soil is a moderately stagnic phaeozem with moderated calcification. The parent material is loess loam above loess. The pH values range from 7.1 to 7.4. For detailed characteristics of the soil profile and for the experimental data see table 6.

The soil at the sampling location Adenstedt is a so-called gray earth. This soil is affected by backwater below 50 cm, which can be recognized by a yellowish-gray coloring due to iron and manganese oxides. Black organic inclusions at a depth of about 40 cm as a consequence of vegetation fires are a special characteristics of this soil. This loess (loam over loess) consists of strongly clay silt down to 75 cm depth which obstructs the vertical drain of excess rain water (seeping water). The increase of the $^{129}I/^{127}I$ ratios for depths between 60 cm and 75 cm can be explained by these hydrological conditions. The organic substances at a depth of about 40 cm influence the migration behavior. At this depth, a constant $^{129}I/^{127}I$ ratio is observed (Fig. 2) and, in

particular, the ^{129}I concentrations decline more slowly than expected. Thus, it appears that free ^{129}I is exchanged for ^{127}I adsorbed at the organic material.

It follows that organic material is an iodine accumulator with low thermodynamic stability which ensures high iodine mobility. A similar behavior of iodine was already discussed in other studies [18, 19].

The high ^{127}I concentrations over the entire soil depth are also remarkable. Similarly high ^{127}I concentrations were observed only for the soil of Groß Lobke. The very slow decline of the ^{127}I concentrations within both soil profiles indicates that the lowest iodine migration rates occur in these soils. The small $^{129}I/^{127}I$ ratios support this explanation.

4.7 Field Groß Lobke

The sampling location Groß Lobke [7, p. 252-254] is a field with crop rotation of wheat, wheat, sugar beets. The soil is a luvic phaeozem with small clay differences. The parent material is sand loess over sand strip loess over loess. The pH values were between 6.9 and 7.3. For detailed characteristics of the soil profile and for the experimental data see table 7.

As observed for the soil Adenstedt, the soil at Groß Lobke exhibits by a brownish color precipitations of iron and manganese oxides around vertically directed roots. The rust tubes become smaller with decreasing water saturation. They appear below 100 cm depth at Adenstedt and below 150 cm at Groß Lobke. This oxidative process leads to the transformation from yellow loess to yellow-brown loess loam. The oxidation-reduction potential increases and, consequently, the iodine migration can be slowed down due to transformation of iodide into iodate which has smaller diffusion lengths and which can form surface bound oxides. This leads to a slower migration.

This process requires a pH value in the range from 5 to 6, where iodate is not stable. The iodine POURBAIX-Diagram [20] of the oxidation-reduction potentials versus pH values in soils [21] gives an oxidation-reduction potentials of 0.76 V for the borderline between stable iodide and stable iodate at pH 5. It decreased down to 0.64 V at pH 7. Therefore, iodate can only be formed in soils with high pH values. The maximum oxidation-reduction potentials occurring in soils are close to 0.8 V. This is the case at Adenstedt and Groß Lobke and makes in connection with their high pH values the low observed iodine migration rates in these soils Adenstedt and Groß Lobke plausible. Moreover, the biological activity increases in the soil with increasing pH value, so that more water-insoluble organic complexing agents are formed.

A special characteristic is a very deep reaching A horizon in the soil Groß Lobke. It is characterized by earthworm activity (in German: Wurmhumus Axh-horizon). With a depth of over 40 cm this A horizon reaches below the usual ploughshare depth of maximal 35 cm. Moreover, deep plowing does not dig up the soil completely. Thus it appears that the plateau-like $^{129}I/^{127}I$ ratios in the upper soil (Fig. 2) are not necessarily the result of soil cultivation. The iodine concentrations are dominated by the dynamic process of the accumulation – dependent on soil characteristics – within the upper soil zone. The fact that the boundary of the earthworm stamped A horizon can be

recognized in depth dependence of the ^{129}I concentrations (Fig. 3), shows that even at the borderline to the water-saturated soil zone (Sw-horizon) the dynamics of the accumulation is sufficient to enrich ^{129}I. The increase of the $^{129}I/^{127}I$ ratios in the depth range between 90 cm and 140 cm is due to the higher clay content in the Bt horizons. The soil Groß Lobke is the soil with the lowest $^{129}I/^{127}I$ ratio in the lower soil zone. However, the measured $^{129}I/^{127}I$ ratio of $(5.4 \pm 0.5) \times 10^{-11}$ exceeds the lowest measured pre-nuclear ratio of $(5.7 \pm 1.1) \times 10^{-12}$ [6] still by an order of magnitude. Thus, the anthropogenic ^{129}I has reached the deepest sampling interval between 200 cm and 250 cm. Also the ^{129}I concentrations here are significantly higher than in the soils from Barum, Ricklingen and Twenge.

5 Migration and Accumulation

5.1 Discussion of the ^{129}I and ^{127}I depth profiles

The iodine concentration in the soil is the result of wet and dry deposition of atmospheric iodine, which in the case of ^{127}I originates from the sea. For the soils of Lower Saxony, ^{127}I was introduced over thousands of years during the entire history of the soils starting with the melting of the ice masses after the last ice age (late Weichsel-glacial). During that time the ^{127}I was in equilibrium with natural ^{129}I with an isotopic ratio of presumably 10^{-12}. The fallout of anthropogenic ^{129}I occurred on a completely different, much shorter time scale, namely since the 1940s. Thus, the time scales of the input of the two iodine isotopes differ by up to 14000 years.

But in any case, due to the phenomena of downward migration and upward accumulation (as described in chapter 5.2) the residence times of ^{127}I and ^{129}I in the upper soil horizons are long enough to transform ^{127}I and ^{129}I into the same chemical species. Consequently, identical chemical speciation and physical properties of ^{127}I and ^{129}I can be assumed over the entire soil column. The dynamic process of the migration for both nuclides depends on the concentration gradients of the entire iodine (^{127}I) which was adjusted over thousands of years and which can be assumed to represent a chemical long-term equilibrium state. However, different depth dependences are observed for ^{127}I and ^{129}I (comp. Fig. 3).

As a consequence of the different transport processes involved in the migration of iodine in the soils, the long-term fallout of ^{127}I is expected to result in an exponential decrease of concentrations over the depth of the soil. The surface-projected ^{127}I concentrations are coarsely in agreement with this expectation (Fig. 3). For ^{129}I one observes exponential decreases in the upper and lower soil zones which, however, exhibit different values of their characteristic depths (Fig. 3).

The differing depth distributions of ^{127}I and ^{129}I in the soils are the result of different adjustment of the adsorption-desorption equilibrium. This equilibrium is adjusted in dynamic processes between the iodine species bound to the soil and dissolved in the fluids over the entire fall-out time. Differences in the iodine concentrations in the run-off and seeping water lead to concentrations gradients, shortly called equilibrium concentration gradients. A material transfer along these gradients can, however, only occur with the iodine which is dissolved or loosely bound and which

takes part in the transport processes and not that part of the iodine which is strongly adsorbed to the soil matrix. The measured iodine concentrations contain both parts of iodine and cannot distinguish between the migrating from the bound parts which do not take part in the adjustment of the steady-state equilibrium.

The (surface-projected) iodine concentrations presented in Figs. 3 only show apparent processes of migration. The differences in the depth dependencies are the result of the different fall-out time-scales of ^{127}I and ^{129}I and the various sorption, migration, and accumulation mechanisms which can occur on these time scales. For ^{127}I, transport processes which allow sorption and desorption on time scales above 50 years are relevant and cause in each depth-profile an equalization of the slope in the different soil horizons. For the transport of anthropogenic ^{129}I, only those processes are relevant which occur on time-scales of less than 50 years. This results in completely different depth dependencies of the ^{127}I and ^{129}I concentrations.

The ^{127}I depth profiles decrease with depth approximately exponentially with different characteristic lengths. For ^{129}I one observes a steep decrease below the surface. For depths between 30 and 70 cm the slopes flatten followed by an approximately exponential decrease with depth. The differences in the depth profiles of ^{127}I and ^{129}I can be interpreted in terms of the individual soil characteristics. These differences become even more pronounced in the depth profiles of the ^{129}I/^{127}I ratios. A sharp decline of the ^{129}I/^{127}I ratios is observed between 30 cm and 70 cm depth in all seven profiles (Fig. 2). It always occurs at the borderlines between the water-saturated and the water-unsaturated soil zones.

Immobilization of ^{129}I is only possible if exchange between the bound ^{127}I in the soil and the free ^{129}I in the soil water is possible on the time-scale of the fall-out. The likelihood of this exchange is determined by the absolute ^{129}I/^{127}I ratio of the free iodine taking into account possible co-adsorbing species and the reversibility of the adsorption. The reversibility of the adsorption is given by the thermodynamic stability of the adsorbate, i.e. of the formation of the complex between the adsorbing agent and the adsorptive. Adsorbates which are more stable in the thermodynamic sense form preferentially and exhibit the smallest reversibility.

Because of the longer interaction times and the higher concentration of ^{127}I compared to ^{129}I, ^{127}I preferentially occupies the thermodynamically favorable sorption places. Without newly generated sorption places, which can lead to an irreversible ^{129}I adsorption, virtually no irreversible adsorption and immobilization of ^{129}I can take place (comp. Fig. 4).

The relative portion of reversible binding places is substantially higher for ^{129}I than for ^{127}I on the time-scale of the anthropogenic ^{129}I fall-out. Therefore, the trace ^{129}I possesses a higher mobility than the total stable ^{127}I. The higher ^{129}I mobility compared to that of the total iodine causes the different values of the characteristic lengths in the upper and lower soil zones (Fig. 3). The reversibility of the adsorption is the crucial factor ruling the distribution of the iodine between the fluid and the soil matrix. Thermodynamically unstable sorption is characterized by sorption energies of less than 60 kJ mol^{-1}. Such sorption processes are called physical sorption [10]. Physical sorption is not specific with respect to adsorbed ions. The lowest sorption energies for physical

sorption of iodine are equivalent to the atomic effective cohesion energy of 7.11 kJ mol^{-1} [11]. This type of sorption occurs via adherence and condensation processes at phase boundary layers. It is about one tenth of the maximum physical sorption energies.

For the distribution of a trace element in an adsorbing medium the diffusion through boundary layers is crucial. Diffusion boundary layers occur at different places and have different qualities in the water-saturated (lower soil) and water-unsaturated soil zones (upper soil). The three-phase system of soil air, soil water, and soil matrix makes an effective immobilization of iodine possible in the upper soil zone via alternating drains and refills of pores. Here, the crucial factor is the sequence between precipitation and dry periods. For this situation the KELVIN equation applies which connects the surface tension (contact angle) at maximum pore filling with pore size. This explains the hydrodynamical dispersion on the basis of distribution of pore sizes and the texture of the soil. Differences in the saturation of the pores with water as a result of the pore size distribution influence the sorption in phase boundary layers only in the upper, water-unsaturated soil zone.

In the water-saturated lower soil zone, there is just a two-phase system of soil water and soil matrix. Since the pores are usually water-saturated an effective immobilization of iodine occurs here as a consequence of diffusion. Moreover, the generation rate of new irreversible adsorption places is smaller in the lower soil zone because of the decrease of chemical and biological activity and the increase of mineralization in the soil with increasing depth.

Thus, is appears that reversible adsorption places, which favor immobilization of ^{129}I, are missing in the lower soil zone. The lower soil offers more thermodynamically stable adsorption places at minerals. This chemical adsorption has sorption energies from approximately 60 kJ mol^{-1} up to 450 kJ mol^{-1} [10]. However, these adsorption places are already occupied by ^{127}I. This results in an increasing mobility of the anthropogenic ^{129}I with increasing soil depth which reaches maximum values in the water-saturated soil zone. The larger characteristic lengths of the ^{129}I profiles in the upper soil zone point to a slower migration and a more efficient accumulation which is attributed to reversible sorption.

5.2 Accumulation of traces in the soil

The iodine concentration gradient between precipitation and soil permits only dislocation (migration) of iodine into deeper soil layers. Accumulation of water-soluble components in the precipitation is not possible without a loss of water from soils. The loss of soil water results, however, in the soil from evaporation and transpiration (evapotranspiration) [12]. Evapotranspiration is on the annual average responsible for a loss of water from the soil into the atmosphere of more than 45% of the precipitation [13, 14], transpiration from plants being much more efficient than evaporation. Differences in the vegetation influence strongly the actual evapotranspiration and consequently the migration of water-flexible traces in the soil [12]. Basically and essentially the depth of the roots determine the ascendancy of the migration in the upper or lower soil. It results an short circuit current water flow between the soil water and the root zone. Because of this, only a variable part of the precipitation reached the water-saturated soil zone.

The quantity of water escaping by evapotranspiration from the upper soil zone is recharged via capillary forces which cause a capillary rise of water from deeper soil zones or precipitation. The resulted short circuit current water flow in combination with evapotranspiration leads to accumulation of water-soluble substances originating from precipitation in the upper soil zone. With increasing water saturation, i.e. with increasing depth and increasing depth of the roots, accumulation becomes less important in comparison to migration because of decreasing capillary rise. With increasing water in the deeper soil, accumulation of traces is no longer possible.

Depending on the hydrological conditions, these depths of short-circuit-current water flow are reached between 30 cm and 70 cm in the soil profiles investigated. This is reflected in Fig. 2 in the sharp decline of the $^{129}I/^{127}I$ ratios and in the ^{129}I concentrations (Fig. 3) as in a general change of the characteristic depths. It does not appear for ^{127}I (Fig. 3) for which chemical sorption dominates. The thickness of this accumulation layer is equal to the height of capillary rise. Only in the layers where capillary rise occurs, accumulation is possible. Differences in the vegetation cover and in the local hydrology influence the thickness of the layer with capillary rise and cause a high variability of the evapotranspiration, on the one hand, and the competition between accumulation and migration in the soils, on the other. The plateau-like $^{129}I/^{127}I$ ratios in layers where capillary rise occurs (Fig.2) are mainly a consequence of accumulation and not necessarily due to soil cultivation operations. The characteristics of the individual soils discussed in chapter 4 confirm these statements.

6 ^{129}I and ^{127}I deposition densities

After fall-out situations, the surface-projected concentrations A_F according to eq. 1, integrated from a maximum depth d_{max} of 40 cm or 60 cm to the surface, are frequently discussed in term of deposition densities arguing that most of the radionuclides observed are still in the upper layers of the soil profile. We shall discuss this issue in the context of the observations made in this work for the iodine isotopes. The assumption that the surface-projected concentrations represent deposition densities depends on the condition that no significant iodine loss occurred into deeper depths. This condition does, however, not hold true in the case of ^{127}I because of its long input time. The observed surface-projected concentrations of ^{127}I range from 2.3 g m^{-2} to 7.2 g m^{-2} with a geometric mean of 3.5 g m^{-2} and a geometric standard deviation of 1.6. The annual deposition density of ^{127}I as determined from the analysis of precipitation in Lower Saxony is of the order of a few mg m^{-2} a^{-1} [5, 6], only. Consequently, no large local variation of the long-term integral of ^{127}I is to be expected and we attribute this variability to losses of ^{127}I out of the depth columns investigated over.

Also the similarly high variability of the surface-projected concentrations of ^{129}I contradicts the assumption that they represent deposition densities. Given the precipitation situation at the investigated locations, also the ^{129}I deposition densities should be similar. But again, we observe a wide range of values from 118 mBq m^{-2} to 390 mBq m^{-2}, with a geometric mean of 168 mBq m^{-2} and a geometric standard deviation of 1.5. Also the differences in the vegetation cover and the consequent different evapotranspiration conditions do not sufficiently explain these differences.

From ^{129}I data in wet precipitation collected in open fields [6] we calculate a mean integral deposition ^{129}I density of approximately 100 mBq m^{-2} for the last 50 years. In this number the contribution from dry deposition is not included. As demonstrated by the different ^{127}I and ^{129}I concentrations in open-field and through-falling precipitation [6] this contribution is important. The through-falling rain contains a contribution of dry deposition washed up from the canopies of trees. The ^{129}I activity concentrations in the through-falling rain were higher than in open-field precipitation by factors between 3.5 and 4.7 [6]. This dry deposition results from the sedimentation of aerosols onto the canopies and from the filtering of the air by the vegetation. The sedimentation depends strongly on the size of the particles, while the filtering does not. From this it follows that an estimation of the dry deposition is not possible from the difference between open field and through-falling precipitation. A comparison of the ^{129}I deposition densities of forest location Eilenriede with other sampling locations suggest, however, just a small influence of the air filtering of forests.

All ^{129}I deposition densities determined from the analysis of soil profiles is supposed to be too small. It must be assumed that the difference of the average ^{129}I deposition density to the maximum ^{129}I deposition density (222 mBq m^{-2}) was lost out of the sampling areas, with the exception of the soil with the maximum ^{129}I deposition density (pasture Vestrup). A reason for that is that the highest ^{129}I concentrations were determined in the lower soil zone of the soil profile with the highest ^{129}I deposition density (pasture Vestrup). Although the ^{129}I concentrations in the lower soils do not contribute considerably to the total deposition density, even the highest ^{129}I deposition density can be evaluated only as a lower limit of the ^{129}I fall-out. The small ^{129}I concentrations in the water-saturated soil zones do represent another quality for the determination of the deposition density than the ^{129}I concentrations in the water-unsaturated soil zones since in the saturated soil zone losses may have occurred which cannot be accounted for.

The measured ^{129}I concentrations depend on the equilibrium concentration gradient between the different soil zones. There are distinct differences in the material transport in the upper and the lower soil zone which have to be taken into account when determining deposition densities from soil depth profiles. Material transfer is highly variable in the water-unsaturated upper soil zone and shows little local and temporal variation in the water-saturated lower soil zone. This implies an effective discharge through-flow in the lower soil zone. The material flow in the upper soil zone occurs through an unsteady (up/down) flow rate of capillary water. Therefore, the upper soil zone acts as storage medium for traces and gives rise in combination with evapotranspiration to accumulation. For iodine, a considerable material loss from of the sampled area is caused in the lower soil zone by the stationary flow of water containing small concentrations of the iodine. For the calculation of deposition densities, the ^{129}I concentrations of the water-unsaturated upper soil zone can be integrated as they are, but the concentrations in the lower soil zones need to be corrected for an unknown loss of iodine. The small ^{129}I concentrations in the lower soil zone can not be neglected. This is demonstrated e.g. by the $^{129}I/^{127}I$ ratios in the lower soil zones observed for the fields Twenge and Barum which increase at depth due to a limited vertical downward flow of water (Fig. 2).

The differences between the "^{129}I deposition densities", calculated according to equ. 1, can only be understood when the soil characteristics are taken into account (see chapter 4). However, a

comparison of the "^{129}I deposition densities" obtained for Lower Saxony with those determined for soils from Zhitomir/Ukraine and from Moscow/Russia [5, 15] (far-off nuclear installations and not significantly affected by the Chernobyl fall-out) is nevertheless meaningful, because the ^{129}I deposition densities differ by factors between 3 and 10. Thus, there is a much higher ^{129}I contamination of the soils in Lower Saxony than in these regions of Russia and Ukraine (see table 8).

7 Conclusions

The depth distribution of ^{127}I and ^{129}I has been investigated in seven soil profiles from Lower Saxony/Germany down to depths of up to 250 cm. Both nuclides in the soil originate from dry and wet deposition of iodine compounds from the atmosphere. The observed ^{129}I/^{127}I isotopic ratios clearly prove that ^{129}I at all depth is anthropogenic. The ^{127}I concentration depth profiles are the result of a continuous input over thousands of years, while the fall-out of man-made ^{129}I occurred during the last 50 years, only. There are characteristic differences in the depth dependencies of ^{127}I compared to those of ^{129}I at each sampling location as well as between the different locations. These differences can be understood when the characteristics of the individual soils is taken into account, the respective hydrodynamical conditions, and the different time scales on which the fallout of the isotopes occurred. Based on this understanding the relevance of the different soil characteristics for the migration of iodine can be rated.

Two soil zones have to be distinguished for the interpretation of the migration of the iodine isotopes, the upper water-unsaturated soil zone and the lower water-saturated soil zone. In the upper zone, a three phase system exists, which consists of soil matrix, soil water, and soil air, in which the dissolved iodine species are transported by the capillary water. The vertical flow of water is rapidly changing, both in direction and intensity, and drying out of the upper soils leads to accumulation of dissolved traces. In the lower soil zone, there is only a two phase system of soil matrix and soil water. Vertical and horizontal transport of water can remove dissolved traces from the volume sampled. In these systems, the migration of the iodine species is a dynamic process. Its velocity depends also on the hydrodynamical dispersion on the thermodynamic stability of adsorption processes which connect the iodine to stationary water phases or to the soil matrix and thus hinder the transport to deeper depths. One has to distinguish in this context between an unspecific physical sorption from specific chemical sorption processes, the latter having much higher sorption energies and consequently higher thermodynamical stability.

The differences observed in the depth dependencies of ^{129}I and ^{127}I concentrations, can be understood as a result of the differences in the timescales during which the two isotopes were brought into the soil. Over very long times, ^{127}I was introduced to the soils and during this time an equilibrium state has been achieved in the soil profiles. All the thermodynamically stable adsorption places are pre-occupied by the old iodine, presumably with a pre-nuclear ^{129}I/^{127}I isotopic ratio of about 10^{-12}. When ^{129}I and ^{127}I from fresh or recent fallout with an ^{129}I/^{127}I isotopic ratio of up to 10^{-6} are introduced into the soil, the migration of the new iodine species is slowed down by unspecific physical sorption processes only. As a consequence, the man-made ^{129}I appears to

migrate faster as the bulk of the stable iodine which consists of the large amount of old iodine and a trace of recent ^{127}I. Also other processes, such as accumulation of ^{129}I in the upper soil zones due to evapotranspiration, are influenced by the competition between the old iodine occupying the more stable sorption places and the recent one which is more mobile due to its unspecific sorption. When in addition the individual soil characteristics and hydrodynamical conditions at the sampling locations are taken into account, the observed depth profile of ^{129}I and ^{127}I can be consistently understood.

It appears that the anthropogenic ^{129}I was not completely retained or accumulated within the upper soil zones. Significant portions of ^{129}I might have migrated into lower soil horizons and into the groundwater and thus were removed from the sampled soil volumes. The ^{129}I concentrations integrated over the depth of the profiles are at best first order estimates of the integral ^{129}I deposition densities of the fall-out, because the migration of the traces of ^{129}I is accelerated in the water-saturated soil zones and may have led to significant ^{129}I losses which cannot be quantified. Large differences in the fall-out of ^{129}I can, however, be distinguished on the basis of these first order estimates. This is e.g. the case if one compares the deposition densities in Lower Saxony/Germany with those in Moscow/Russia, Zhitomir/Ukraine and locations in northern Ukraine highly affected by fall-out from the Chernobyl accident.

Besides the loss of ^{129}I from the sampled volume, the degree of accumulation in the upper soil zone is crucial for the interpretation of depth-integrated ^{129}I concentrations in terms of deposition densities. Its influence can be estimated by evaluation of the evapotranspiration on the basis of vegetation cover. Closed vegetation surfaces increase the apparent ^{129}I deposition densities as a function of the capillary rise by accumulation in the first 30 cm depth. Crucial for the determination of deposition densities from soil profiles is the thickness of the upper soil zone where capillary rise occurs and evapotranspiration and hydrodynamical conditions in the lower and upper soil zones which determine the capillary rise rates. On the basis of the results of this investigation and taking all these factors into account, predictions of favorable sampling locations for the determination of deposition densities from the analysis of soil profiles can be made. This is e.g. relevant for investigations of ^{129}I within soils with the goal of retrospective dosimetry of past exposures to ^{131}I.

8 Outlook

The scenario discussed here for the system of ^{129}I and ^{127}I is also generally applicable to other nuclides if the role of competing ions is taken into consideration which influence sorption processes and consequently migration and accumulation. So the situation of ^{137}Cs and potassium is e.g. similar to that of ^{129}I and ^{127}I, respectively. This was observed also in the depth profiles investigated in this work [22]. Potassium can be used as a proxy for the total quantity of Cs-like nuclides including the omnipresent ammonium. It fulfils all the functions attributable to ^{127}I in this work if one replaces the $^{129}I/^{127}I$ ratios with the $^{137}Cs/^{40}K$ ratios [21]. The Cs-K-system is more complicated since the competing ammonium has to be taken into account. Because of the special chemical and physical characteristics of iodine, the only non-isotopic ion competing in the adsorption of iodine is nitrate if it is present in high concentrations.

The phenomenological explanation of migration, sorption and accumulation of trace substances in soils presented here considers a multitude of different physical and chemical effects which themselves are influenced by many factors. It goes far beyond the approaches of leaching and impact experiments. Models of the migration of trace substances have to consider all these physical and chemical effects. Consequently, it is not astonishing that physical models, such as multi-compartment models, convection dispersion models and simple transfer models do not satisfactorily reproduce the distribution of radionuclides in soils [23]. They have to be scrutinized on the basis of the results presented her in order to accomplish a better understanding of the migration of trace substances in soils.

Acknowledgements

This work was funded by the German Science Foundation (DFG, Bonn) and The Swiss National Fond (SNF). We are grateful to the Paul Scherrer Institute (PSI) and the Swiss Federal Institute of Technology (ETH) who jointly operate the Zurich AMS facilities.

References

1 J. E. Moran, U. Fehn, Ray T. D. Teng, Variations in $^{129}I/^{127}I$ ratios in recent marine sediments: evidence for a fossil organic component, Chemical geology 152 (1998) 193 - 203.

2 D.R. Schink, P.H. Santschi, O. Corapcioglu, U. Fehn, Prospects for "iodine-129 dating" of marine organic matter using AMS, Nucl. Instr. Meth. Phys. Res. B 99 (1995) 524 - 527.

3 A. Schmidt, Ch. Schnabel, J. Handl, D. Jakob, R. Michel, H.-A. Synal, J.M. Lopez, M. Suter, On the analysis of iodine-129 and iodine-127 in environmental materials by accelerator mass spectrometry and ion chromatography. Sci. Total Environ. 223 (1998) 131 - 156.

4 R. Michel, Th. Ernst, S. Szidat, Ch. Schnabel, H.-A. Synal, Langfristige Entwicklung von Iod-129 in der Umwelt, Klausurtagung des Radioökologieausschusses der SSK 25./26.7.2001 in Klais, Berichte der Strahlenschutzkommission (2002) in press.

5 S. Szidat, A. Schmidt, J. Handl, D. Jakob, W. Botsch, R. Michel, H.-A. Synal, C. Schnabel, M. Suter, J.M. López-Gutiérrez, W. Städe, Iodine-129: Sample preparation, quality control and analyses of pre-nuclear materials and of natural waters from Lower Saxony, Germany. Nucl. Instr. Meth. Phys. Res. B172 (2000) 699 - 710.

6 S. Szidat, Iod-129: Probenvorbereitung, Qualitätssicherung und Analyse von Umweltmaterialien. Ph.D. thesis, University Hanover (2000). Available at: http://edok01.tib.uni-hannover.de/edoks/e002/32217211X.pdf.

7 Mitteilungen der Deutschen Bodenkundlichen Gesellschaft, Exkursionsführer Band 90 (1999) ISSN-0343-107x, Deutsche Bodenkundliche Gesellschaft.

8 E. Boaretto, D. Berkovits, R. Delmas, R.R. Johnson, A. Kaufman, M. Magaritz, M. Paul, M. Pourchet, Measurements of anthropogenic radionuclides in environmental samples, Nucl. Instr. Meth. Phys. Res. B92 (1994) 350 - 356.

9 T. Ernst, S. Szidat, J. Handl, D. Jakob, R. Michel, Ch. Schnabel, H.-A. Synal, F.J. Santos Arevalo, I. Benne, J. Boess, J. Böttcher, E. Gehrt, A. Capelle, J. Schneider, W. Schäfer, ^{129}I und ^{127}I in europäischen Böden, in: R. Michel, M. Täschner, A. Bayer (eds.) Praxis des Strahlenschutzes: - Messen, Modellieren, Dokumentieren -, Tagungsband der 34. Jahrestagung des Fachverbandes für Strahlenschutz e.V., Kloster Seeon, 21. - 25. April 2002, TÜV-Verlag, Köln (2002) 167 - 174.

10 R. Kümmel, E. Worch, Adsorption aus wäßrigen Lösungen, Deutscher Verlag für Grundstoffindustrie Leipzig (1990) 19.

11 A. F .M. Barton (ed.) Handbook of solubility parameters and other cohesion parameters, CRC 2nd Edition (1991) N5,04.

12 H. Ernstberger, Einfluß der Landnutzung auf Verdunstung und Wasserbilanz, Verlag Beiträge zur Hydrologie, Kirchzarten (1987) 6 - 29.

13 H. Hellmann, Lehrbuch der Hydrologie Band 2: Qualitative Hydrologie – Wasserbeschaffenheit und Stoff-Flüsse, Gebrüder Borntraeger (1999) 51 - 52.

14 P. Krahe, M. Glugla, Abfluß und Wasserbilanz der Bundesrepublik Deutschland. Information 1/96 Bundesanstalt für Gewässerkunde Berlin-Koblenz, cited in [13].

15 A. Schmidt, ^{129}I und stabiles Iod in Umweltproben Qualitätskontrolle von Analysenmethoden und Untersuchungen zur Radioökologie und zur retrospektiven Dosimetrie, Ph. D. thesis, University Hanover (1998). Available at: http://edok01.tib.uni-hannover.de/edoks/e002/245403892l.pdf.

16 A. Geller, Handbuch Mikrobiologische Bodenreinigung, Schriftenreihe Materialien zur Altlastenbearbeitung, Band 7, Landesanstalt für Umweltschutz Baden-Württemberg (1991) Kap. 2.4.2.2 online: http://www.uvm.baden-wuerttemberg.de/alfaweb/berichte/abstracts/band07.html.

17 F. Scheffer, P. Schachtschabel et al., Lehrbuch der Bodenkunde, 14. Aufl. Ferdinand Enke Verlag Stuttgart (1998) 56 - 58 /129, 202 - 203.

18 M. Schäfer, Iod-Dynamik im Boden. Ph. D. thesis, TU München (1994) 121-133.

19 E. Pel, Zum Verhalten von Iod im System Boden-Pflanze-Luft, KfK 5118 (1993) 57 - 58, 81 - 82.

20 H. J. M. Bowen, Environmental Chemistry of the Elements, Academic Press (1979) 26, cited in [19] 72.

21 Th. Ernst, Anthropogenes Iod-129 als Tracer für Umweltprozesse, Ein Beitrag zum Verhalten von Spurenstoffen bei der Migration in Böden und beim atmosphärischen Transport. Ph.D. thesis, University Hanover (2003) in preparation.

22 S. Harb, Ph. D. thesis, University Hanover (2003) in preparation.

23 G. Kirchner, Transportprozesse von Spurenstoffen in terrestrischen Ökosystemen, Habilitationsschrifft University Bremen (1997) 1 - 8. Available at: http://lmst02.physik.uni-bremen.de/habil.pdf.

The authors of this publication

T. Ernst, S. Szidat*, J. Handl, D. Jakob, R. Michel, Center for Radiation Protection and Radioecology, University Hanover, Am Kleinen Felde 30, D-30167 Hannover, Germany, E-mail Corresponding author: michel@zsr.uni-hannover.de

Ch. Schnabel**, Laboratory for Radiochemistry and Environmental Chemistry, University Bern, Freiestrasse 3, CH-3012 Bern, Switzerland

Ch. Schnabel**, F.J. Santos Arevalo, Institute for Particle Physics, ETH Hoenggerberg, CH-8093 Zurich, Switzerland

H.-A. Synal, Paul Scherrer Institute, c/o Institute for Particle Physics, ETH Hoenggerberg, CH-8093 Zurich, Switzerland

Benne, J. Boess, E. Gehrt, A. Capelle, J. Schneider, State Geological Survey of Lower Saxony (NLfB), Stilleweg 2, D-30655 Hannover, Germany

W. Schäfer, NLfB Soil-Technological Institute, Friedrich-Mißler-Straße 46/48, 28211 Bremen, Germany

J. Böttcher, Institute of Soil Science, University Hanover, Herrenhäuser Straße 2, 30419 Hannover, Germany

**present address:* Laboratory for Radiochemistry and Environmental Chemistry, University Bern, Freiestrasse 3, CH-3012 Bern, Switzerland

***present address:* Scottish Universities Environmental Research Center, Scottish Enterprise Tech. Park East Kilbride G75 0QF, United Kingdom

Figure and table captions

Fig. 1. Sampling locations in Lower Saxony

Fig. 2. $^{129}I/^{127}I$-isotopic ratios in seven soil profiles from Lower Saxony

Fig. 3. Surface-projected activity concentrations of ^{129}I (upper graph) and surface-projected concentrations of ^{127}I (lower graph) of seven soil profiles from Lower Saxony.

Fig. 4. Scheme illustrating the different sorption mechanisms, their energies and isotopic interchange rates. The different input histories of ^{129}I and ^{127}I cause different isotopic compositions of iodine in the four sorption regimes.

Table 1: Soil characteristics, ^{129}I activity concentrations, ^{127}I concentrations, and $^{129}I/^{127}I$ isotopic ratios of the soil profile „pasture Vestrup“.

Table 2: Soil characteristics, ^{129}I activity concentrations, ^{127}I concentrations, and $^{129}I/^{127}I$ isotopic ratios of the soil profile „forest Eilenriede“.

Table 3: Soil characteristics, ^{129}I activity concentrations, ^{127}I concentrations, and $^{129}I/^{127}I$ isotopic ratios of the soil profile „lawn Ricklingen“.

Table 4: Soil characteristics, ^{129}I activity concentrations, ^{127}I concentrations, and $^{129}I/^{127}I$ isotopic ratios of the soil profile „field Barum“.

Table 5: Soil characteristics, ^{129}I activity concentrations, ^{127}I concentrations, and $^{129}I/^{127}I$ isotopic ratios of the soil profile „field Twenge“.

Table 6: Soil characteristics, ^{129}I activity concentrations, ^{127}I concentrations, and $^{129}I/^{127}I$ isotopic ratios of the soil profile „field Adenstedt“.

Table 7: Soil characteristics, ^{129}I activity concentrations, ^{127}I concentrations, and $^{129}I/^{127}I$ isotopic ratios of the soil profile „field Groß Lobke“.

Table 8: Surface-projected (activity-) concentrations and corresponding $^{129}I/^{127}I$ isotopic ratios of soil profiles investigated in this work in comparison with those obtained from other locations.

Corresponding author:

Prof. Dr. Rolf Michel

Zentrum für Strahlenschutz und Radioökologie, Universität Hannover

Am Kleinen Felde 30, D-30167 Hannover, Germany

Tel: +49-(0)511-762-8683, FAX: +49-(0)511-762-3319, email: michel@zsr.uni-hannover.de

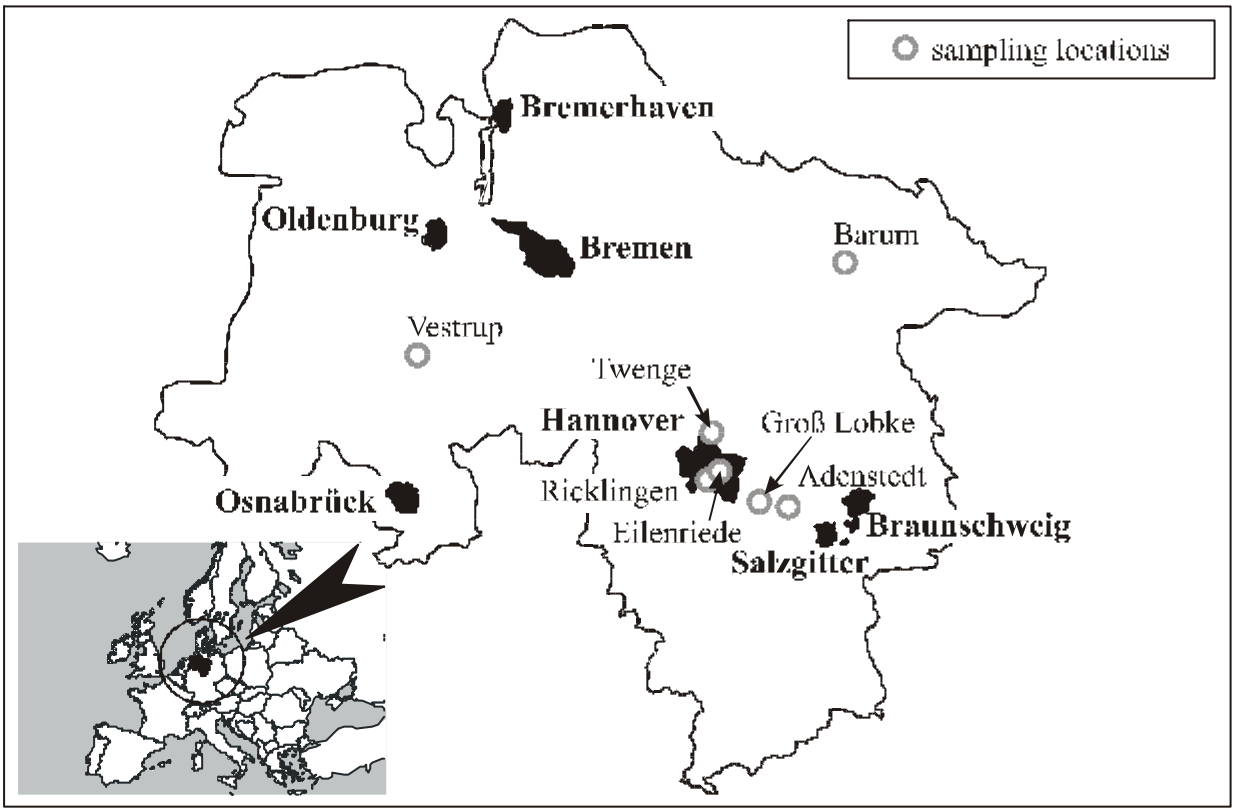
sampling locations
Bremerhaven
Oldenburg
Bremen
Barum
Vestrup
Twenge
Hannover
Groß Lobke
Adenstedt
Osnabrück
Ricklingen
Eilenriede
Braunschweig
Salzgitter

Fig. 1

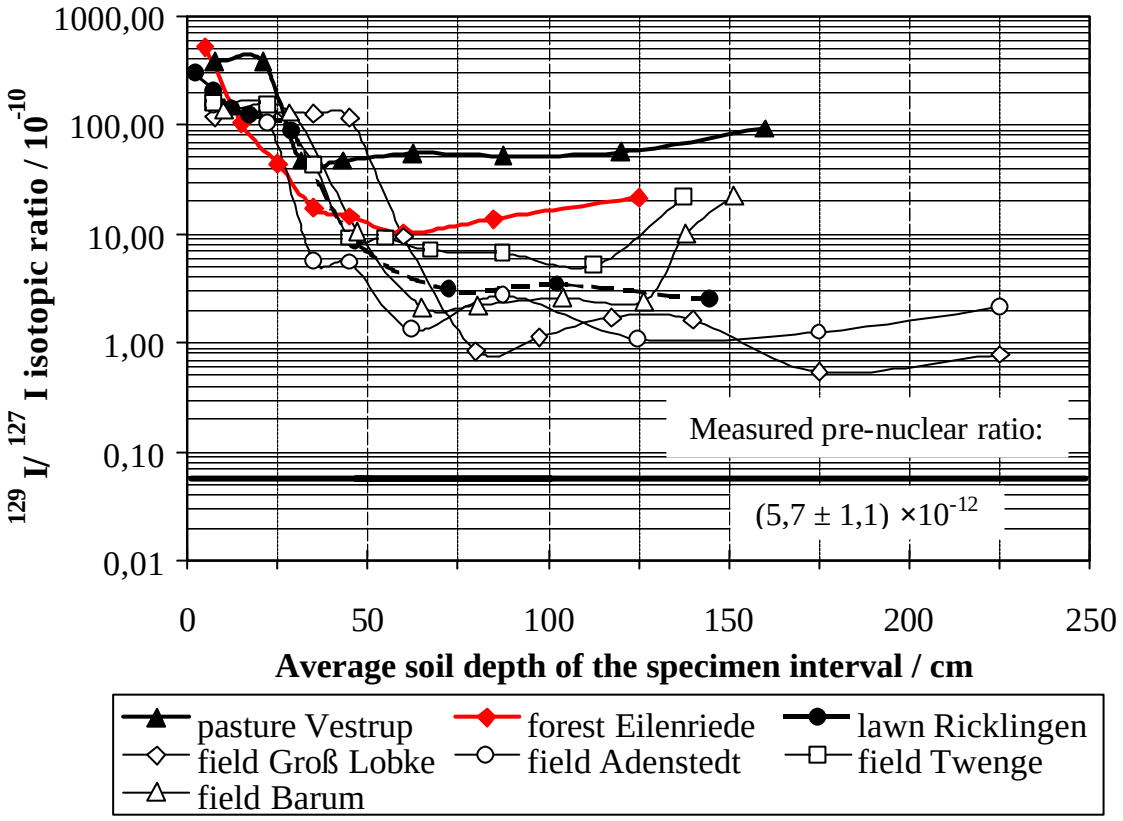
1000,00
100,00
10,00
1,00
0,10
0,01
129 I/ 127 I isotopic ratio / 10-10
Measured pre-nuclear ratio:
(5,7 ± 1,1) ×10-12
0
50
100
150
200
250
Average soil depth of the specimen interval / cm
pasture Vestrup
forest Eilenriede
lawn Ricklingen
field Groß Lobke
field Adenstedt
field Twenge
field Barum

Fig. 2

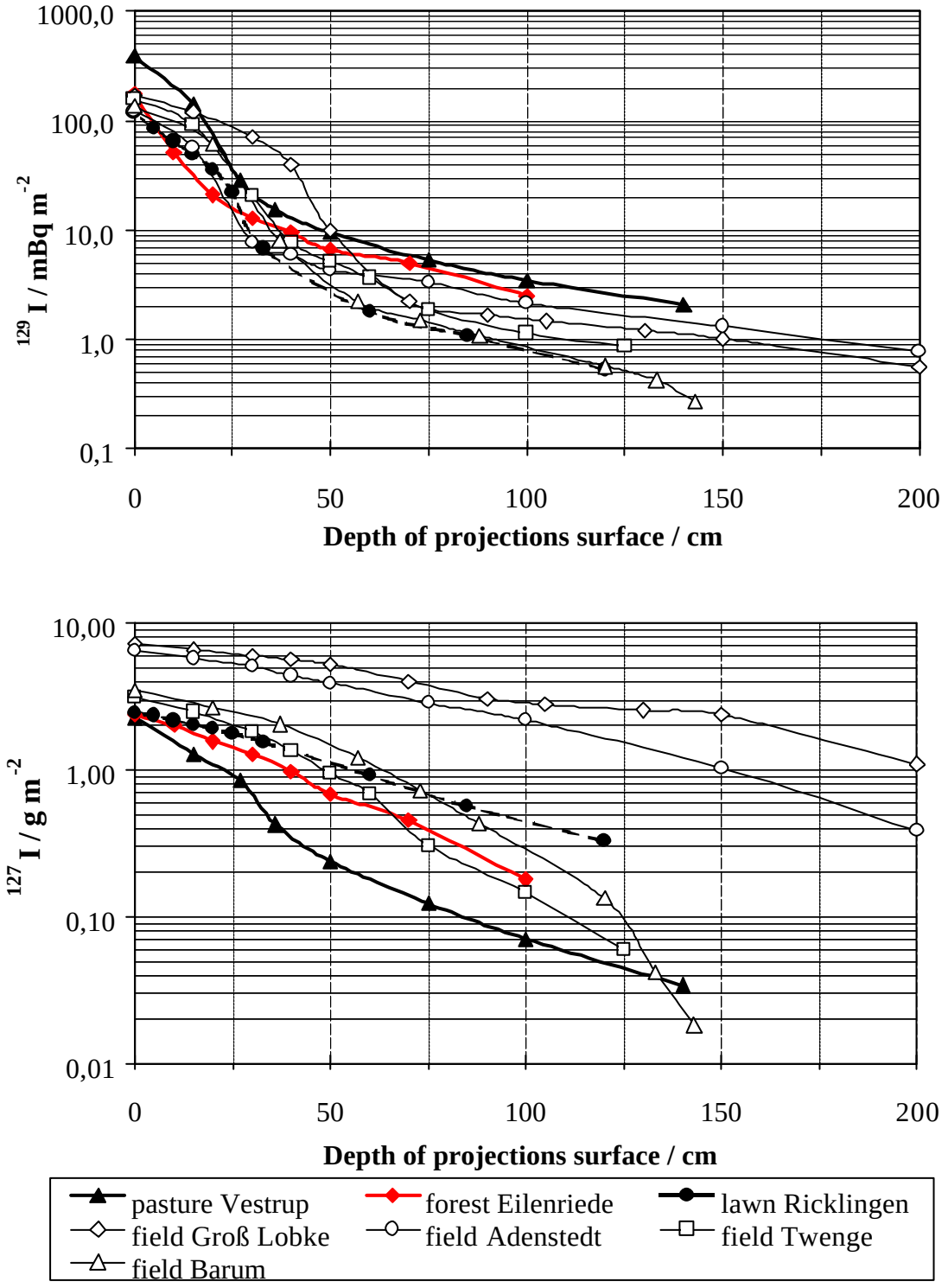
1000,0
100,0
10,0
1,0
0,1
129 I / mBq m-2
0
50
100
150
200
Depth of projections surface / cm
10,00
1,00
0,10
0,01
127 I / g m-2
0
50
100
150
200
Depth of projections surface / cm
pasture Vestrup
forest Eilenriede
lawn Ricklingen
field Groß Lobke
field Adenstedt
field Twenge
field Barum

Fig. 3

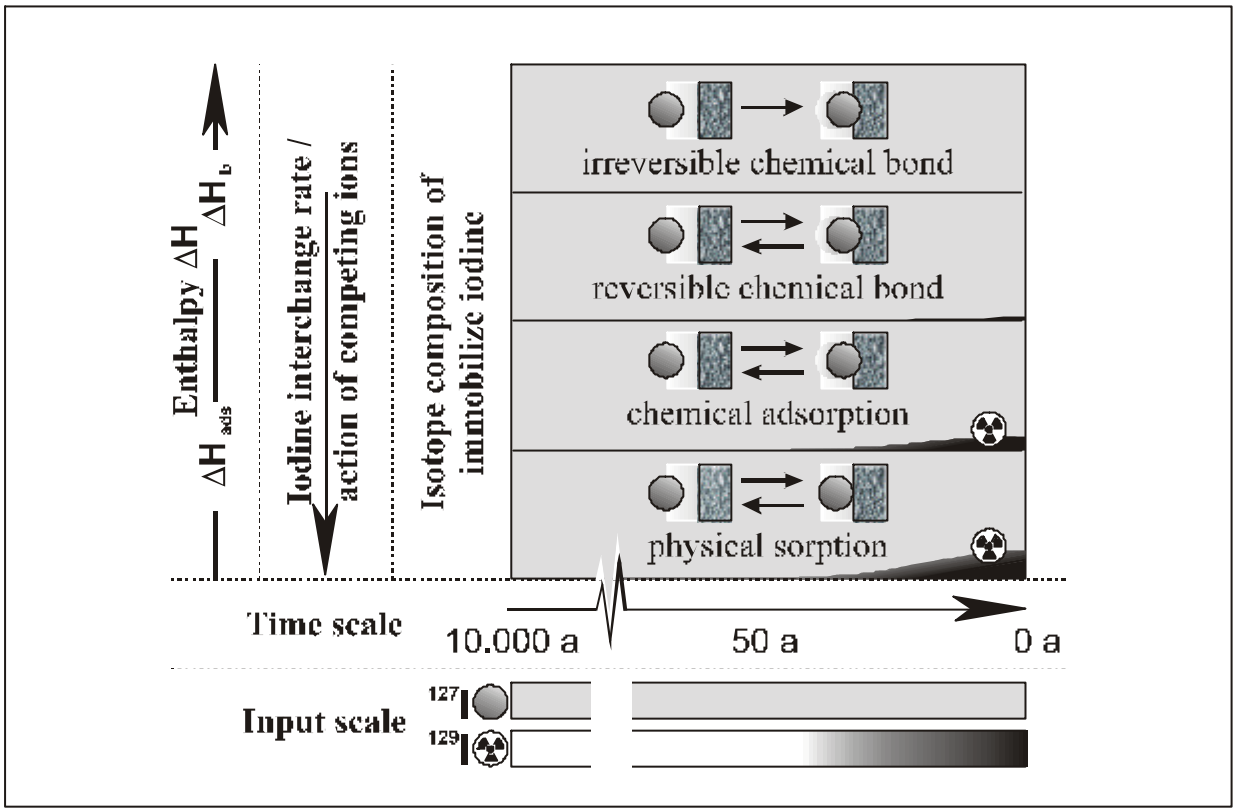
Enthalpy ΔH
ΔH_b
ΔH_ads
Iodine interchange rate /
action of competing ions
Isotope composition of
immobilize iodine
irreversible chemical bond
reversible chemical bond
chemical adsorption
physical sorption
Time scale
10.000 a
50 a
0 a
Input scale
127
129

Fig. 4

Table 1:

sampling interval	horizon german	horizon FAO	texture	characteristics	sand	silt	clay	bulk density	^{129}I	^{127}I	$^{129}I/^{127}I$ isotopic ratio
cm	[7]				%	%	%	g cm^{-3}	nBq g^{-1}	mg kg^{-1}	$\times 10^{-10}$
0-15	rAep +Aeh	Ahp	sand weak silty, greatly weak pebbly	reddish dark brownish gray, intense humous, minor compactness of the packing, very weakly minted crumble structures, reddish brown,	81.2	13.9	4.9	1.2 ± 0.1	1413 ± 46	5.6 ± 0.4	378 ± 26
15-27	Bsh	Bhs		medium humous , intense iron blotched, middle compactness of the packing, weak salient coherent structures	83.0	12.8	3.9	1.2 ± 0.1	748 ± 24	3.0 ± 0.2	376 ± 28
27-36	Bhs		sand weak silty, weak pebbly	dull brown, medium iron blotched, middle compactness of the packing, weak salient coherent structures bright reddish brown, weak iron blotched, middle compactness of the packing, particulate structure, partly coherent structures; up to 45 cm sand medium clay, greatly weak pebbly partly sand medium clay, brownish bright gray, partly beige, middle compactness of the packing, particulate structure, partly coherent structures	82.3	13.9	3.8	1.4 ± 0.1	102 ± 3	3.3 ± 0.2	46.8 ± 3.2
36-50	Bs - Sw	Bs			77.4/ 66.1	18.5/ 24	4.1/ 9.9	1.5 ± 0.2	28 ± 1	0.9 ± 0.1	46.9 ± 6.7
50-75	Sw	Bcr	sand intense clay, greatly weak pebbly and stony	Greenish bright gray, weak iron blotched, middle compactness of the packing, greenish bright gray, intense iron blotched, high compactness of the packing, diaclase fill of sand weak silty, coherent structures	70.4	12.6	17	1.5 ± 0.2	11.3 ± 0.4	0.3 ± 0.1	54.6 ± 18.5
75-100	Sw							1.4 ± 0.1	5.2 ± 0.2	0.2 ± 0.1	52.1 ± 37.9
100-140	Go-Sd Go			nutty aggregates of fine sand weak silty, bright reddish brown, medium iron blotched, middle compactness of the packing	72.2	12	15.8	1.6 ± 0.2	2.1 ± 0.1	0.06	56.0
140-180	Go/				74.2	10.8	15	1.5 ± 0.2	3.5 ± 0.1	0.06	92.5
160-180	Gro				71.4	15.6	13				

Table 2:

sampling interval	horizon german	horizon FAO	texture	characteristics	sand	silt	clay	bulk density	^{129}I	^{127}I	$^{129}I/^{127}I$ isotopic ratio
cm	[7]				%	%	%	g cm^{-3}	nBq g^{-1}	mg kg^{1}	$\times 10^{-10}$
+1	L	Oi	leave mulch								
+1	Of	Oa									
0-10	Aeh	Ah	coarse sandy medium sand	greatly weak pebbly and stony, brownish gray, medium humous , middle compactness of the packing	97.7			1.5 ± 0.2	1117 ± 36	3.2 ± 0.2	521 ± 33
10-20	Aeh		medium clay sand, greatly weak pebbly and stony	brown gray, medium humous , middle compactness of the packing	76.1	13.4	10.5	1.4 ± 0.1	237 ± 8	3.5 ± 0.2	103 ± 6
20-30	Ah-Go			yellow brown, greatly weak humous , greatly weak iron blotched, middle compactness of the packing	80.3	12.0	7.7	1.4 ± 0.1	60.3 ± 2.1	2.2 ± 0.1	43.7 ± 3.0
30-40		B1						1.4 ± 0.1	25.2 ± 0.9	2.2 ± 0.1	17.2 ± 1.1
40-50	Go-Sw			gray yellow, weak iron blotched, middle compactness of the packing	83.8	8.8	7.4	1.4 ± 0.1	21.2 ± 0.8	2.2 ± 0.1	14.4 ± 1.0
50-70	Go-Swd	B2	coarse sandy medium sand	marmorate, medium iron blotched, high compactness of the packing	97.4			1.3 ± 0.1	5.7 ± 0.2	0.8 ± 0.1	10.1 ± 1.1
					97.3						
70-100								1.3 ± 0.1	6.1 ± 0.3	0.7 ± 0.1	13.7 ± 1.5
100-150	Gro		sandy clay loam	greatly weak pebbly and stony, gray, weak iron blotched, middle compactness of the packing	72.8	14.0	13.3	1.1 ± 0.1	3.3 ± 0.2	0.23 ± 0.06	21.2 ± 5.8

Table 3:

sampling interval	horizon german	horizon FAO	texture	characteristics	sand	silt	clay	bulk density	^{129}I	^{127}I	$^{129}I/^{127}I$ isotopic ratio
cm	[7]				%	%	%	g cm^{-3}	nBq g^{-1}	mg kg^{-1}	$\times 10^{-10}$
0-5	rAp+Ah	Ap1	silty clay sand	dark brown, medium humous middle compactness of the packing	42.9	46.8	10.3	1.3 ± 0.1	489 ± 19	2.5 ± 0.1	297 ± 19
5-10								1.3 ± 0.1	332 ± 14	2.4 ± 0.1	205 ± 14
10-15								1.3 ± 0.1	253 ± 18	2.7 ± 0.1	141 ± 12
15-20								1.2 ± 0.1	208 ± 9	2.6 ± 0.1	122 ± 8
20-25								1.3 ± 0.1	216 ± 9	2.8 ± 0.1	115 ± 7
25-33								1.3 ± 0.1	154 ± 7	2.7 ± 0.1	87.0 ± 5.8
33-60	Al	At2	sandy clay silt	sallow brown, greatly weak humous , middle compactness of the packing	34.2	56.2	9.6	1.4 ± 0.1	13.3 ± 0.8	2.4 ± 0.1	8.5 ± 0.7
60-85	IISw-Bt	Bt1	medium silty sand,	into nests intense clay sand, brownish gray, weak iron blotched, middle compactness of the packing	58.7	32.9	8.4	1.3 ± 0.1	2.2 ± 0.3	1.1 ± 0.1	3.0 ± 0.4
85-120	Sw	B2	weak clay sand	partly medium sand coarse sandy, brownish gray, weak iron blotched, middle compactness of the packing	81.5	13.4	5.1	1.4 ± 0.1	1.1 ± 0.1	0.50 ± 0.04	3.4 ± 0.4
120-170	Sw Sd	B3	medium sand coarse sandy	up to 150cm weak pebbly, brown gray, minor compactness of the packing; up to 170cm sandy clay loam, weak pebbly, partly intense clay sand and weak clay loam, yellow brown, high compactness of the packing	98.3/ 45.2	1.7/ 19.4	0/ 35.4	1.4 ± 0.1	0.8 ± 0.1	0.47 ± 0.04	2.4 ± 0.4

Table 4:

sampling interval	horizon german	horizon FAO	texture	characteristics	sand	silt	clay	bulk density	^{129}I	^{127}I	$^{129}I/^{127}I$ isotopic ratio
cm	[7]				%	%	%	g cm^{-3}	nBq g^{-1}	mg kg^{-1}	$\times 10^{-10}$
0-20	Ap	Ap1	weak clay silt	dark brown gray, weak humous, minor compactness of the packing; alluvial deposits loess	27.1	64	8.9	1.2 ± 0.1	306 ± 8	3.4 ± 0.2	135 ± 7
20-37								1.2 ± 0.1	264 ± 7	3.1 ± 0.2	129 ± 7
37-57	wM	Ahb2	weak clay silt	brown, greatly weak humous , middle compactness of the packing; alluvial deposits loess	21.6	68.2	10.3	1.3 ± 0.1	23.1 ± 0.8	3.3 ± 0.2	10.5 ± 0.6
57-73	Al	Bt1	sandy silt	sallow brown beige, middle compactness of the packing	15	74.4	10.6	1.3 ± 0.1	3.5 ± 0.2	2.5 ± 0.1	2.1 ± 0.2
73-88	Bt	Bt2	clay silt	reddish brown, middle compactness of the packing; sand loess	6.1	73.6	20.3	1.2 ± 0.1	2.3 ± 0.2	1.6 ± 0.1	2.2 ± 0.2
88-120	Bt	Bt3	weak clay sand	sand loess with diffuse inserts of sandy silt, gray brown, middle compactness of the packing	14.7	70.6	14.7	1.2 ± 0.1	13 ± 0.1	0.76 ± 0.04	2.6 ± 0.3
120-133								1.3 ± 0.1	0.9 ± 0.1	0.54 ± 0.03	2.4 ± 0.3
133-143	Bbt-Cv	Bt /C	fine sandy	intense stony; stone level, beige gray, middle compactness of the packing; wind borne sand	79	16	5	1.5 ± 0.2	1.1 ± 0.1	0.16 ± 0.02	9.9 ± 1.6
143-160			medium sand					1.7 ± 0.2	1.0 ± 0.1	0.06 ± 0.01	22.1 ± 5.1

Table 5:

sampling interval	horizon german	horizon FAO	texture	characteristics	sand	silt	clay	bulk density	^{129}I	^{127}I	$^{129}I/^{127}I$ isotopic ratio
cm	[7]				%	%	%	g cm^{-3}	nBq g^{-1}	mg kg^{1}	$\times 10^{-10}$
0-15	Ap	Ap	fine sand medium sand	brownish black, medium humous, minor compactness of the packing coherent structure brownish black, humous, minor compactness of the packing, coherent structures, charcoal and clay bricks	88.7	6	5.3	1.4 ± 0.1	331 ± 12	3.2 ± 0.2	154 ± 9
15-30								1.4 ± 0.1	321 ± 12	3.2 ± 0.2	151 ± 9
30-40								1.3 ± 0.1	101 ± 5	3.6 ± 0.2	42.7 ± 3.0
40-50	E	E			86.2	8.7	5.1	1.3 ± 0.1	19.3 ± 1.2	3.2 ± 0.2	9.0 ± 0.7
50-60	fAe	Bh (Abh)	medium sand fine sandy	dark rust-colored brown, weak humous , middle compactness of the packing				1.4 ± 0.1	11.1 ± 0.7	1.8 ± 0.1	9.0 ± 0.7
60-75	Bs /Bhs			rust-colored brown, middle compactness of the packing	89.1	5.9	4.1	1.3 ± 0.1	9.2 ± 0.7	2.0 ± 0.1	7.0 ± 0.6
75-100	Bs Go	B1	medium sand	yellow gray, weak iron blotched, middle compactness of the packing	91.0	4.9	4.1	1.5 ± 0.2	1.9 ± 0.2	0.44 ± 0.03	6.6 ± 1.0
100-125	Go	Bc2	medium sand coarse sandy	in nutty aggregates silt sandy, yellow gray, in nutty aggregates gray, weak iron blotched, middle compactness of the packing	95.3	3.0	1.7	1.7 ± 0.2	0.7 ± 0.1	0.20 ± 0.05	5.1 ± 1.7
125-150			medium sand	weak pebbly, yellow gray, weak iron blotched, middle compactness of the packing	99.5	0.5	0	1.8 ± 0.2	2.0 ± 0.2	0.14 ± 0.08	21.6 ± 12.3

Table 6:

sampling interval	horizon german	horizon FAO	texture	characteristics	sand	silt	clay	bulk density	^{129}I	^{127}I	$^{129}I/^{127}I$ isotopic ratio
cm	[7]				%	%	%	g cm^{-3}	nBq g^{-1}	mg kg^{1}	$\times 10^{-10}$
0-15	Axp	Ahp	intense clay silt	dark gray, medium humous , minor compactness of the packing	6.8	75.9	17.3	1.2 ± 0.1	380 ± 17	3.9 ± 0.3	148 ± 14
15-30								1.2 ± 0.1	282 ± 13	4.1 ± 0.3	103 ± 8
30-40	Axh			gray, middle compactness of the packing	5.4	77.7	16.9	1.3 ± 0.1	14.1 ± 0.6	3.9 ± 0.2	5.5 ± 0.4
40-50	Sw	B1		yellowish gray, to be riddled with black, medium iron blotched, middle compactness of the packing	3.6	75.8	20.6	1.2 ± 0.1	14.0 ± 0.6	3.9 ± 0.3	5.5 ± 0.4
50-75								1.2 ± 0.1	3.1 ± 0.2	3.6 ± 0.3	1.3 ± 0.1
75-100	Sw		medium clay silt, yellowish gray, marbled with ocher, weak iron blotched	fine laminated iron precipitation around Roots, medium carbonate containing, middle compactness of the packing	3.0	77.0	20	1.2 ± 0.1	4.0 ± 0.2	2.3 ± 0.2	2.7 ± 0.3
100-150	fGo+ICkc -Sw / fGo+ICc	Br2 /Cr			4	84	12	1.2 ± 0.1	1.4 ± 0.1	1.9 ± 0.2	1.1 ± 0.2
150-200	fGo+ICv-Sw	Cr		partly iron precipitation around Roots, medium carbonate containing, medium compactness of the packing	8.1	82.7	9.2	1.3 ± 0.1	0.8 ± 0.1	1.0 ± 0.2	1.2 ± 0.3
200-250	fGo+ICv-Sd		weak clay sand	partly medium sand up to medium silty clay, downward increasing, weak silty clay, bright gray, greatly weak carbonate containing	45.7	41.1	13.2	1.4 ± 0.1	1.1 ± 0.1	0.80 ± 0.18	2.1 ± 0.5

Table 7:

sampling interval	horizon german	horizon FAO	texture	characteristics	sand	silt	clay	bulk density	^{129}I	^{127}I	$^{129}I/^{127}I$ isotopic ratio
cm	[7]				%	%	%	g cm^{-3}	nBq g^{-1}	mg kg^{-1}	$\times 10^{-10}$
0-15	Alp	Ahp	sandy clay silt	dark brown gray, weak humous, minor compactness of the packing	32.3	54.5	13.2	1.3 ± 0.1	268 ± 11	3.4 ± 0.2	118 ± 8
15-30								1.2 ± 0.1	264 ± 10	3.0 ± 0.2	131 ± 8
30-40	Axh-Al				31.5	55.1	13.5	1.2 ± 0.1	267 ± 11	3.2 ± 0.2	125 ± 8
40-50	Sw-Axh-Bht Sw-Bht		silty clay sand	partly weak silty sand, dirty brown, greatly weak humous , greatly weak iron and manganese blotched, concretions, middle compactness of the packing	35.3	49.6	15	1.3 ± 0.1	236 ± 9	3.1 ± 0.2	115 ± 7
50-70		Bht1						1.5 ± 0.2	25.8 ± 1.1	4.1 ± 0.2	9.4 ± 0.6
70-90	Sw-Bht		weak clay silt	with 2 cm intensely Layer of intense clay medium sand, gray ocher blotched, partly black, greatly weak humous, medium iron blotched removable with weak clay medium sand, gray dark ocher marbled, medium iron blotched, middle compactness of the packing	69.4	17.8	12.7	1.3 ± 0.1	2.1 ± 0.2	3.8 ± 0.2	0.8 ± 0.1
90-105								1.4 ± 0.1	1.0 ± 0.1	1.4 ± 0.1	1.1 ± 0.1
105-130					18.1	70.1	11.8	1.2 ± 0.1	0.9 ± 0.1	0.75 ± 0.04	1.7 ± 0.2
130-150	Sw-Bhtv	Bt2			65.7	25.4	9	1.3 ± 0.1	0.8 ± 0.1	0.71 ± 0.04	1.6 ± 0.2
150-200	Sw / fGo+Sw			with 1 cm intense Layer of clay sand, yellowish gray, medium iron blotched, medium carbonate containing, indurations in the loess, minor compactness of the packing	7	82	11	1.3 ± 0.1	0.7 ± 0.1	2.0 ± 0.1	0.5 ± 0.1
200-250	Sw /Sd	Br3		yellowish gray, weak iron blotched, medium carbonate containing, minor compactness of the packing up to 225 cm sandy clay silt, greatly weak pebbly and stony, medium carbonate containing, minor compactness of the packing, up to 265 cm weak silty clay, dark gray, high compactness of the packing	37.5/ 32.5	50.2/ 62.9	12.4/ 62.9	1.4 ± 0.1	0.8 ± 0.1	1.6 ± 0.1	0.8 ± 0.1

Table 8:

sampling location and soil utilization	^{129}I mBq m^{-2}	^{127}I g m^{-2}	$^{129}I/^{127}I$ isotopic ratio
pasture Vestrup	390 ± 50	2.3 ± 0.5	2.6×10^{-08}
forest Eilenriede	178 ± 26	2.4 ± 0.4	1.1×10^{-08}
lawn Ricklingen	118 ± 25	2.5 ± 0.4	7.2×10^{-09}
geometric mean, permanent closed vegetation	$201 \times 1.6^{\pm 1}$	$2.4 \times 1.03^{\pm 1}$	1.3×10^{-08}
field Twenge	158 ± 20	3.1 ± 0.5	7.5×10^{-09}
field Barum	136 ± 16	3.5 ± 0.4	5.8×10^{-09}
field Adenstedt	124 ± 16	6.4 ± 1.1	2.8×10^{-09}
field Groß Lobke	171 ± 23	7.2 ± 0.9	3.5×10^{-09}
geometric mean, fields	$146 \times 1.2^{\pm 1}$	$4.8 \times 1.5^{\pm 1}$	4.6×10^{-09}
geometric mean, all profiles	$168 \times 1.5^{\pm 1}$	$3.5 \times 1.6^{\pm 1}$	7.1×10^{-09}
geometric mean, all profiles except pasture	$146 \times 1.2^{\pm 1}$	$3.8 \times 1.6^{\pm 1}$	5.7×10^{-09}
Zhitomir, Ukraine. 1997 [5]	$38 \times 1.7^{\pm 1}$	-	-
forest Moscow, Russia 1996 [15]	$49 \times 1.5^{\pm 1}$	-	-
pre-nuclear, Russia, 1939 [5]	0.084 ± 0.017	-	-